

Electron-irradiation effects on monolayer MoS₂ at elevated temperatures

Carsten Speckmann^{1,2,*}, Kimmo Mustonen¹, Diana Propst^{1,2},
Clemens Mangler¹, and Jani Kotakoski^{1,*}

¹University of Vienna, Faculty of Physics, Boltzmannngasse 5,
1090 Vienna, Austria

²University of Vienna, Vienna Doctoral School in Physics, Boltzmannngasse 5,
1090 Vienna, Austria

*Email: carsten.speckmann@univie.ac.at and jani.kotakoski@univie.ac.at

(Dated: November 6, 2024)

The effect of electron irradiation on 2D materials is an important topic, both for the correct interpretation of electron microscopy experiments and for possible applications in electron lithography. After the importance of including inelastic scattering damage in theoretical models describing beam damage, and the lack of oxygen-sensitivity under electron irradiation in 2D MoS₂ was recently shown, the role of temperature has remained unexplored on a quantitative level. Here we show the effect of temperature on both the creation of individual defects as well as the effect of temperature on defect dynamics. Based on the measured displacement cross section of sulphur atoms in MoS₂ by atomic resolution scanning transmission electron microscopy, we find an increased probability for defect creation for temperatures up to 150°C, in accordance with theoretical predictions. However, higher temperatures lead to a decrease of the observed cross sections. Despite this apparent decrease, we find that the elevated temperature does not mitigate the creation of defects as this observation would suggest, but rather hides the created damage due to rapid thermal diffusion of the created vacancies before their detection, leading to the formation of vacancy lines and pores outside the measurements field of view. Using the experimental data in combination with previously reported theoretical models for the displacement cross section, we estimate the migration energy barrier of sulphur vacancies in MoS₂ to be 0.47 ± 0.24 eV. These results mark another step towards the complete understanding of electron beam damage in MoS₂.

I. INTRODUCTION

Understanding electron beam damage in (scanning) transmission electron microscopy [(S)TEM] is of the utmost importance to distinguish between observed intrinsic effects and effects driven by the imaging process, as well as to implement these insights for example in electron beam lithography [1–3]. While electron beam damage has been investigated for decades [4, 5], a detailed quantification has only been possible since the advent of two-dimensional (2D) materials [6]. An often neglected additional factor for these investigations is chemical etching, which can occur due to a non-ideal vacuum within the microscope or because of sample contamination [7]. Previous studies on electron beam damage have focussed on a variety of 2D materials such as graphene [8–10], hexagonal boron nitride [11–14], MoS₂ [15–17], MoSe₂ [18, 19] and phosphorene [20, 21]. However, only recently the role of inelastic scattering was included into theoretical models for electron beam damage in non-conducting 2D materials [16, 17, 22], while previous reports only tried to estimate its importance indirectly [23, 24]. Following these reports, other studies were centred on the effect adatoms have on the displacement process [25], as well as to measure the cross sections of different layers in multilayer samples [26] to get a more complete picture of the atomic displacement mechanisms.

It has been reported that fewer defects appear in MoS₂ during STEM imaging above temperatures of 400°C [27]. However, other reports have rather found that sulphur

vacancies agglomerate in vacancy lines, than stay as single or double vacancies [19, 27–31]. In addition, a tendency for pore formation has also been reported at higher temperatures [28–30]. The formation of these defect structures is attributed to the high mobility of sulphur vacancies at elevated temperatures based on thermal diffusion [28, 29, 32]. It was also suggested that defects being created within the field of view (FOV) due to knock-on damage rapidly migrate out of the FOV [28, 32]. Finally, grain boundaries and other vacancy lines were also observed to migrate across the sample [29]. The migration barrier for sulphur vacancies in MoS₂ was calculated by theory with a value of 2.3 eV for an isolated vacancy [33, 34], while adjacent vacancies can lower the energy barrier down to only 0.8 eV [31, 33]. An experimental estimate based on the migration of domain boundaries gives a migration barrier of 0.6 eV [35]. Others have also theorized about the possible migration of adatoms across the sample, filling created vacancies [30]. However, a systematic and quantitative study on the effect of temperature on the creation and migration of defects under electron irradiation has not been carried out yet.

In this work, we measure the displacement cross section of S atoms in MoS₂ at temperatures up to 550°C using scanning transmission electron microscopy at acceleration voltages of 60 and 90 kV. At a temperature of 150°C, the displacement cross section increased compared to its room temperature value [17], which is in agreement with theoretical models attributing this to a thermal activa-

tion of phonons, increasing the maximum transferred energy of the beam electrons to the material [8–10, 36]. However, at higher temperatures the measured cross section decreases significantly. We attribute the apparent decrease to thermal diffusion of sulphur vacancies before they can be detected with the microscope. We use the difference in experimental and theoretical cross sections to estimate the migration energy barrier of sulphur vacancies in MoS₂ to be 0.47 ± 0.24 eV, which is in good agreement with previous theoretical calculations [31, 33] and experimental estimates [35]. Overall, our results show that elevated temperatures do not mitigate defect creation by electron irradiation, but only obscure the effects of the electrons impinging on the sample due to thermal diffusion. These results mark another step towards the complete understanding of electron beam damage in MoS₂, which is important for any future device fabrication.

II. RESULTS AND DISCUSSION

For this work, MoS₂ samples were grown via chemical vapour deposition and were subsequently transferred onto Fusion AX heating chips from Protochips (see the Methods section for more details). To distinguish the effects of the increased temperatures on both the elastic and inelastic scattering damage, two electron energies were used, 60 keV for the mostly inelastic scattering damage regime and 90 keV for the pure elastic scattering damage regime. Temperatures used during the course of this study are 150°C, 300°C, 450°C, 550°C and 750°C and a heating rate of 5°C/s was used for all experiments. Note that no data could be recorded at 750°C as the sample decomposed at this temperature before any measurements could be conducted. This is in good agreement with a previous report identifying the decomposition of MoS₂ in ultra-high vacuum (UHV) to take place between 700°C and 800°C [37].

Measurements on the displacement cross section of MoS₂ were conducted in the same way as reported in our previous study [17], resulting in similar image series of high-angle annular dark field (HAADF) images. In each of these image series, sulphur vacancies were identified and the number of created vacancies per frame was calculated. This was then correlated with the beam current to calculate an average value for the created vacancies per electron impinging on the sample, \bar{N} , which can be converted into the displacement cross section, $\sigma = \bar{N}/\rho$ (see Methods section for more details). Here, ρ indicates the areal density of the sulphur sites in MoS₂, which in this case is identical to the inverse unit cell area, calculated using a lattice constant of 3.19 Å [38], as a single vacancy was assumed to have been created first whenever a double vacancy was observed. The resulting statistics of this analysis for each set of measurements are shown in Fig. 1 with the top row depicting the measurements at 60 keV and the bottom row the measurements at 90 keV.

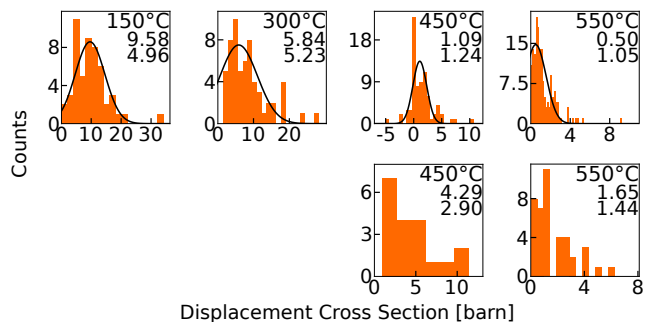


Figure 1. **Statistics of sulphur vacancy formation at elevated temperatures.** Histograms show the statistics of the measured displacement cross sections for different electron energies and temperatures. The top row shows experiments carried out with an electron energy of 60 keV, while the bottom row shows results from experiments carried out at 90 keV. Temperatures are stated in the top right corner of each histogram. Here, one count represents the results of a single image series. The solid lines correspond to fits of a normal distribution to the datasets recorded at 60 keV with means \bar{x} and standard deviations Δx of each fit given in the top-right corner of each plot underneath the temperatures. The values stated for the datasets recorded at 90 keV correspond to the mean and standard deviation of the individual values.

Here, each count corresponds to the calculated displacement cross section based on a single image series. The temperature at which the respective measurements were carried out is indicated in the top right corner of each histogram. Similar to our previous study [17], a Gaussian distribution was fitted to the shown statistics in the top row with the means \bar{x} and standard deviations Δx visible underneath the temperatures. No Gaussian distribution could be fitted to the data acquired at 90 keV, thus, the mean of the individual values and its standard deviation are stated in the histograms instead. Note that no liable data could be recorded at an electron energy of 90 keV below temperatures of 450°C as a pore would always emerge within the field of view after just a single frame, making it impossible to estimate the number of missing atoms.

The cross section values as well as two theoretical models are plotted as a function of temperature in Fig. 2. The models shown here were reported in our previous study [17], including both elastic and inelastic scattering damage into account for the explanation of beam damage in MoS₂ with two distinct ways of incorporating the inelastic scattering processes. The ionization model, describes the inelastic scattering as electron impact ionization, while the excitation model describes the inelastic contributions as valence excitation instead. Both models explain the experimentally observed datapoints reasonably well, with only the ionization model resulting in a quantitatively good agreement with previous reports on the exciton lifetimes in MoS₂ [17].

In Fig. 2, the experimental values measured at 60 keV (blue) start to increase with increasing temperature, fol-

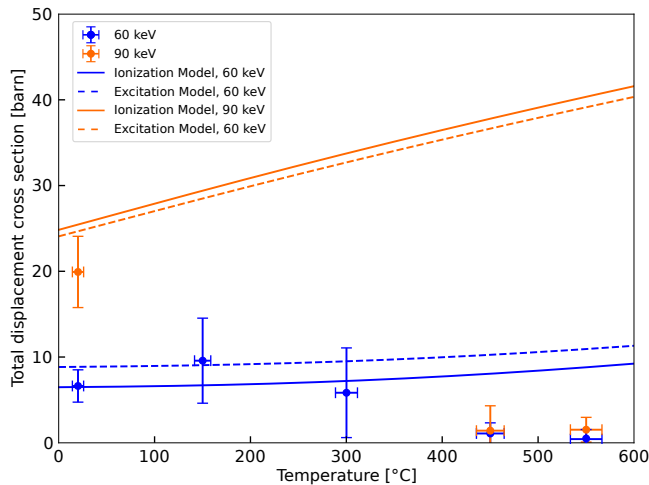


Figure 2. **Experimental displacement cross section values as a function of temperature.** Total displacement cross section values for single sulphur atoms in MoS_2 as a function of temperature measured with electron energies of 60 keV (filled blue circles) and 90 keV (filled orange circles). Room temperature values are taken from Ref. [17]. Lines correspond to theoretical models [17]. The solid lines indicate the impact ionization model with one excited state and the dashed lines indicate the electronic excitation model with two excited states (see Ref. [17] for further details) using the fit parameters stated in Table I of Ref. [17]. Blue lines correspond to an electron energy of 60 keV, while orange lines correspond to an energy of 90 keV.

lowing the predictions of the models. This increase can be described by the thermal activation of phonons that influence the maximum transferable energy of the electron to the S atom [8–10, 36]. A similar trend is also expected for 90 keV electrons, which could however not be measured due to the immediate appearance of a pore, rather than individual sulphur vacancies. However, a decrease in cross section can be observed at temperatures above 150°C, completely deviating from the theoretical models above 300°C, especially for an electron energy of 90 keV (orange). A possible explanation for the decrease of the apparent cross section is the filling of vacancies due to migrating atoms on the sample surface [30], similar to Gr [39]. Another possibility would be a reduction of the inelastic scattering cross section due to the faster recombination of excitations at elevated temperatures, which would however not explain a similar reduction of the cross section within the purely elastic scattering regime (90 keV). However, the most prominent cause for the apparent reduction of the cross section seems to be thermal diffusion [28, 32], as shown in Fig. 3.

Fig. 3(a-e) show an example image series recorded at an acceleration voltage of 60 keV and at a temperature of 550°C. Fig. 3a shows a clean patch of MoS_2 enclosed by contamination, while a small pore including a metal cluster is partially visible at the top left corner of the image. The following three images were recorded at the

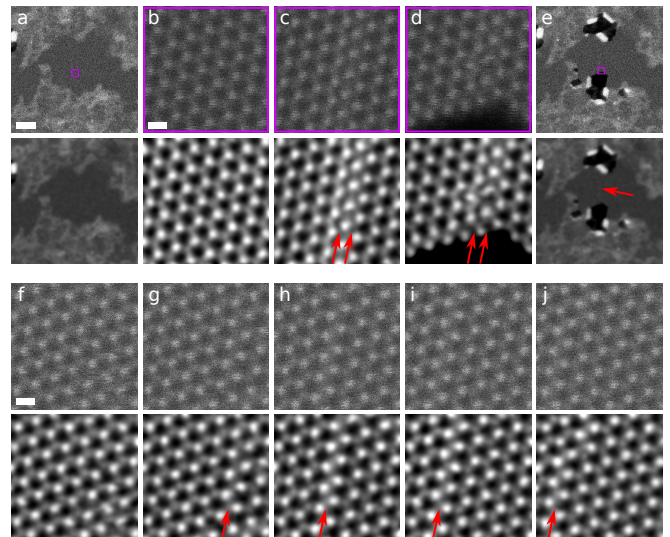


Figure 3. **Example STEM-HAADF image series of MoS_2 at elevated temperatures and the migration of vacancy lines.** Panels (a-e) show five images of an image series where each frame is a $512 \text{ px} \times 512 \text{ px}$ image recorded within a frame time of 0.88 s. Images were taken at an acceleration voltage of 60 keV and at a temperature of 550°C. Images in the top row are as-recorded, whereas a Gaussian blur (4 px in panels a and e and 8 px in panels b-d) has been applied to the images in the second row. Panels (f-j) show five subsequent images of another image series recorded using the same parameters but at 450°C. Images in the top row are as-recorded, whereas a Gaussian blur of 8 px has been applied to the images in the second row. Red arrows are used to indicate vacancy lines in the MoS_2 lattice and cyan rectangles in panels a and e indicate the positions of the zoomed in images in panels (b-d). The scale bars are 5 nm for images in panels a and e and 3 Å for the other images.

position marked with the cyan squares over a period of 145 s between panels b and d. Note that no individual sulphur vacancies can be seen in these images, as was the case for most images taken at 550°C. Rather than individual vacancies, vacancy lines of various sizes could be observed along the zig-zag (ZZ) directions, highlighted by the red arrows. Fig. 3d then shows that the vacancy line ends with a pore that expands into the FOV over time. The amount of damage created during the duration of the irradiation with the electron beam is shown in Fig. 3e, where several pores can be seen to have emerged outside the FOV of the zoomed-in images recorded in between panels a and e with bright clusters (likely Mo) at their edges. Observations of pores outside the FOV, together with the absence of individual vacancies in many images recorded at 450°C and 550°C indicates that most vacancies created by the electron beam migrate out of the FOV before they can be detected, forming pores and/or vacancy lines. This rapid thermal diffusion might be the most prominent reason for the previously observed decrease of atomic displacements when combining electron irradiation with heating above tem-

peratures of 400°C [27]. Thus, elevated temperatures only obscure the creation of vacancies by electron irradiation, but do not mitigate it. Note that all pores that could be observed during these measurements were (partially) located within the contaminated part of the sample, speaking for the pinning of defects by the contamination. This behaviour might be explained by the fact that sulphur vacancies in MoS₂ have dangling bonds, and are therefore likely to bond to contamination once in contact with it. A similar behaviour has been reported in graphene, where contamination was found to hide defects by accumulating on top of it [7].

The vacancy lines are highly mobile as can be seen in Fig. 3(f-j). Fig. 3f shows an almost perfect hexagonal MoS₂ lattice. In the subsequent images, with a frame time of 0.88 s, a vacancy line can be seen to have migrated into the FOV from outside (Fig. 3g), migrating from right to left. The vacancy line is highlighted with a red arrow. During this process, a transitional state of the migration process can be seen in Fig. 3j in which the vacancy line is spread across two sulphur rows. These line defects can form if sulphur vacancies accumulate along a line, and its width is determined by the number of lines where vacancies are present [28, 33, 40, 41]. Our observations seem to agree with previous theoretical and experimental studies on vacancy lines in MoS₂. They have found a preference for the formation along the ZZ direction [28, 29, 33, 40] with pores and Mo clusters forming at their ends [28, 29]. Furthermore, it has been predicted that vacancy lines can act as channels for the migration of S and Mo atoms towards the forming pore [28] due to a reduction of the diffusion energy barrier [28, 31]. Vacancy lines have also been predicted to locally decrease the electronic band gap of MoS₂ depending on the width of the vacancy line [40–42] up to the point where the vacancy line becomes metallic once four rows of sulphur vacancies are present [41], opening the possibility for defect-engineered devices.

Based on the above presented observations, the difference between the theoretically predicted and experimentally observed cross sections is likely to be primarily caused by migration. Thus, this difference can be used to estimate the migration barrier of sulphur vacancies in MoS₂, which was previously only estimated by theoretical means [31, 33, 34] and by an indirect experimental estimate based on the migration of domain boundaries [35]. As also discussed in our previous study on the migration of carbon adatoms on graphene [39] the number of migration steps μ for the defect taken during one image at a given temperature T is

$$\mu(T) = f_0 t_F \exp\left(\frac{-E_m}{k_B T}\right), \quad (1)$$

where f_0 is the attempted jump frequency, t_F the frame time, E_m the migration energy barrier and k_B the Boltzmann constant. When a vacancy is created within the MoS₂ structure, a certain time t_d passes until this defect can be detected via the electron beam. The spe-

cific time until a defect is detected is determined by the position of said defect in relation to the position of the electron beam and its scan parameters. Without thermal diffusion, each defect will be detected once the electron beam scans across its position, which is assumed for the theoretical models. However, if the vacancy is able to jump due to thermal activation, its position is constantly changing, possibly resulting in the vacancy migrating to a location outside the scanned area before it can be detected. The probability for this to happen is directly proportional to $\mu(T)$. As a result, the ratio of the observed cross section σ_{exp} to the theoretical cross section σ_{theo} will also be proportional to the Boltzmann factor

$$\frac{\sigma_{\text{exp}}}{\sigma_{\text{theo}}} \propto \exp\left(\frac{-E_m}{k_B T}\right). \quad (2)$$

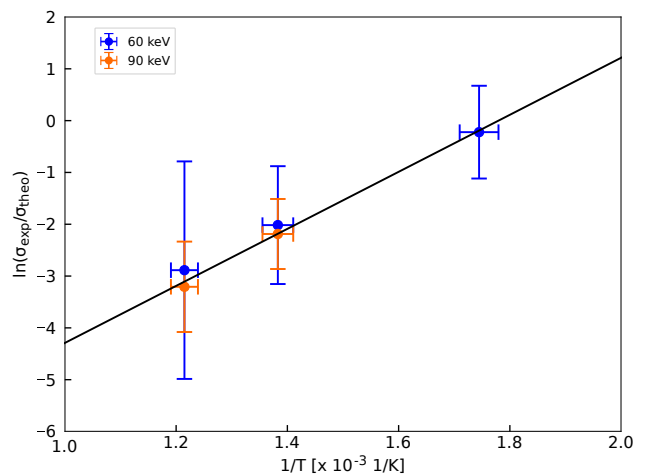


Figure 4. **Ratio of the experimental and theoretical displacement cross section as a function of temperature.** The natural logarithm of the experimentally observed displacement cross sections for single sulphur atoms in MoS₂ normalized to their respective theoretical predictions is plotted as a function of one over temperature while a linear regression is fitted to the datapoints. Blue and orange datapoints correspond to measurements done at electron energies of 60 and 90 keV, respectively.

The corresponding Arrhenius plot is shown in Fig. 4 where a linear regression (black line) is fitted to $\sigma_{\text{exp}}/\sigma_{\text{theo}}$ (blue and orange circles). As the migration of vacancies should only affect the observed cross section values once the observed experimental cross sections are decreasing again, only values recorded above a temperature of 150°C were taken into account. The fit results in a migration energy barrier of 0.47 ± 0.02 eV when using the ionization model and 0.43 ± 0.02 eV when using the excitation model as a theoretical reference. However, the actual uncertainty should be significantly higher due to the uncertainty of the individual datapoints. We estimate the maximum reasonable uncertainty of the migration barrier to be $\sim 50\%$, resulting in values of 0.47 ± 0.24 eV and 0.43 ± 0.22 eV for the ionization and

excitation model, respectively. Both values are in reasonable agreement with the theoretical migration barrier of vacancies next to other vacancies of 0.8 eV [31, 33] and previous experimental estimations based of the migration of domain boundaries of 0.6 eV [35]. As the defects observed during the course of these measurements mostly appear next to each other, it is reasonable to assume that the migration barrier estimated through these measurements is not the pristine energy barrier, but rather corresponds to a defective structure.

III. CONCLUSIONS

In conclusion, our measurements show the effect of elevated temperatures on the observed sulphur displacement cross sections in monolayer MoS₂. While temperatures of up to 150°C result in an increase of the cross section in agreement with theoretical models [8–10, 36], higher temperatures cause a stark decrease in the cross section, deviating from the model predictions. We show that this decrease originates from thermal diffusion of sulphur vacancies out of the field of view before they can be detected. The difference in experimental and theoretical cross sections is used to estimate the migration energy barrier of sulphur vacancies in MoS₂, resulting in a value of 0.47 ± 0.24 eV, which is in good agreement with previous theoretical calculations [31, 33] and experimental estimates [35]. Thus, our results show that elevated temperatures do not mitigate defect creation by electron irradiation, but only obscure the effects of the electrons impinging on the sample. These results mark another step towards the complete understanding of electron beam damage in MoS₂.

METHODS

Sample preparation The MoS₂ sample was grown using chemical vapour deposition (CVD) [43] on a SiO₂ substrate. The MoS₂ was afterwards transferred in air onto a golden transmission electron microscopy grid covered with a holey membrane of amorphous carbon (Quantifoil R 1.2/1.3 Au grid) with a method similar to the one described in Ref. [44]. A tabletop TEM was used to examine the sample and determine areas where a high MoS₂ coverage was present. Afterwards, these identified patches of the sample were transferred onto a Fusion AX heating chip from Protochips. These heating chips were calibrated for each individual chip by the company with

an estimated precision of ± 2 %. The transfer to the heating chip was performed by placing the carbon membrane side of the TEM grid onto the chip and applying a drop of isopropyl alcohol (IPA) to increase adhesion. After the IPA evaporated, the stack was placed on a heating plate for 15 – 20 min at 150°C, after which the grid was ripped off with a vacuum tweezer. This causes parts of the amorphous carbon membrane and the attached MoS₂ to stick to the chip and be ripped off from the Au grid bars. This process was repeated until the predetermined area was successfully transferred onto the heating chip. The sample was loaded into a Nion cartridge and baked overnight at a temperature of 150°C, before being introduced into the microscope magazine storage volume. Measurements were conducted hours to days after the transfer into the magazine storage volume was finished.

Scanning transmission electron microscopy Measurements were carried out using a Nion UltraSTEM 100, an aberration-corrected scanning transmission electron microscope using acceleration voltages of 60 and 90 kV. The probe size of the microscope is ~ 1 Å with a beam convergence semi-angle of 30 mrad and the base pressure inside the microscope column was below 10^{-9} mbar at all times. The instrument is equipped with a cold field emission gun, and images were recorded using a high-angle annular dark field (HAADF) detector with a collection angle of 80 – 300 mrad. Imaging parameters were identical to the ones used in our previous study [17], with a dwell time of 3 μ s/px, a flyback time of 120 μ s and images of 512 px \times 512 px. The resulting frame time is 0.88 s and the time between frames was measured to be 10 ms. Similar to Ref. [17], image series acquisition was stopped as soon as more than two missing S atoms at next-nearest neighbouring lattice sites were observed. Beam currents for both electron energies were measured as described in Ref. [17], resulting in beam currents of 106 ± 3 pA and 196 ± 6 pA for 60 and 90 keV, respectively.

Data analysis The acquired data was analysed in the same way as described in Ref. [17], using a convolutional neural network (CNN) similar to the one used in Ref. [45] optimizing the model created by the CNN by minimizing the intensity difference to the recorded image as described in Ref. [39].

ACKNOWLEDGMENTS

This research was supported by the Austrian Science Fund (FWF) through projects [10.55776/DOC85, 10.55776/P34797] and by the Vienna Doctoral School in Physics.

[1] R. F. W. Pease, *Contemp. Phys.* **22**, 265 (1981), ISSN 0010-7514, URL <https://doi.org/10.1080/>

- [2] T. R. Groves, in *Nanolithography*, edited by M. Feldman (Woodhead Publishing, 2014), pp. 80–115, ISBN 978-0-85709-500-8, URL <https://www.sciencedirect.com/science/article/pii/B9780857095008500038>.
- [3] Y. Chen, *Microelectron. Eng.* **135**, 57 (2015), ISSN 0167-9317, URL <https://www.sciencedirect.com/science/article/pii/S016793171500101X>.
- [4] R. Egerton, P. Li, and M. Malac, *Micron* **35**, 399 (2004), ISSN 09684328, URL <https://linkinghub.elsevier.com/retrieve/pii/S0968432804000381>.
- [5] R. Egerton, *Ultramicroscopy* **127**, 100 (2013), ISSN 03043991, URL <https://linkinghub.elsevier.com/retrieve/pii/S0304399112001763>.
- [6] T. Susi, J. C. Meyer, and J. Kotakoski, *Nat. Rev. Phys.* **1**, 397 (2019), ISSN 2522-5820, URL <http://www.nature.com/articles/s42254-019-0058-y>.
- [7] G. T. Leuthner, S. Hummel, C. Mangler, T. J. Pennycook, T. Susi, J. C. Meyer, and J. Kotakoski, *Ultramicroscopy* **203**, 76 (2019), ISSN 0304-3991, URL <https://www.sciencedirect.com/science/article/pii/S030439911830278X>.
- [8] J. C. Meyer, F. Eder, S. Kurasch, V. Skakalova, J. Kotakoski, H. J. Park, S. Roth, A. Chuvilin, S. Eyhusen, G. Benner, et al., *Phys. Rev. Lett.* **108**, 196102 (2012), URL <https://link.aps.org/doi/10.1103/PhysRevLett.108.196102>.
- [9] J. C. Meyer, F. Eder, S. Kurasch, V. Skakalova, J. Kotakoski, H. J. Park, S. Roth, A. Chuvilin, S. Eyhusen, G. Benner, et al., *Phys. Rev. Lett.* **110**, 239902(E) (2013), URL <https://link.aps.org/doi/10.1103/PhysRevLett.110.239902>.
- [10] T. Susi, C. Hofer, G. Argentero, G. T. Leuthner, T. J. Pennycook, C. Mangler, J. C. Meyer, and J. Kotakoski, *Nat. Commun.* **7**, 13040 (2016), ISSN 2041-1723, URL <https://www.nature.com/articles/ncomms13040>.
- [11] J. C. Meyer, A. Chuvilin, G. Algara-Siller, J. Biskupek, and U. Kaiser, *Nano Lett.* **9**, 2683 (2009), ISSN 1530-6984, URL <https://doi.org/10.1021/nl9011497>.
- [12] C. Jin, F. Lin, K. Suenaga, and S. Iijima, *Phys. Rev. Lett.* **102**, 195505 (2009), URL <https://link.aps.org/doi/10.1103/PhysRevLett.102.195505>.
- [13] J. Kotakoski, C. H. Jin, O. Lehtinen, K. Suenaga, and A. V. Krasheninnikov, *Phys. Rev. B* **82**, 113404 (2010), URL <https://link.aps.org/doi/10.1103/PhysRevB.82.113404>.
- [14] T. A. Bui, G. T. Leuthner, J. Madsen, M. R. A. Monazam, A. I. Chirita, A. Postl, C. Mangler, J. Kotakoski, and T. Susi, *Small* **19**, 2301926 (2023), ISSN 1613-6829, URL <https://onlinelibrary.wiley.com/doi/abs/10.1002/smll.202301926>.
- [15] H.-P. Komsa, J. Kotakoski, S. Kurasch, O. Lehtinen, U. Kaiser, and A. V. Krasheninnikov, *Phys. Rev. Lett.* **109**, 035503 (2012), URL <https://link.aps.org/doi/10.1103/PhysRevLett.109.035503>.
- [16] S. Kretschmer, T. Lehnert, U. Kaiser, and A. V. Krasheninnikov, *Nano Lett.* **20**, 2865 (2020), ISSN 1530-6984, URL <https://doi.org/10.1021/acs.nanolett.0c00670>.
- [17] C. Speckmann, J. Lang, J. Madsen, M. R. A. Monazam, G. Zagler, G. T. Leuthner, N. McEvoy, C. Mangler, T. Susi, and J. Kotakoski, *Phys. Rev. B* **107**, 094112 (2023), URL <https://link.aps.org/doi/10.1103/PhysRevB.107.094112>.
- [18] O. Lehtinen, H.-P. Komsa, A. Pulkin, M. B. Whitwick, M.-W. Chen, T. Lehnert, M. J. Mohn, O. V. Yazyev, A. Kis, U. Kaiser, et al., *ACS Nano* **9**, 3274 (2015), ISSN 1936-0851, URL <https://doi.org/10.1021/acsnano.5b00410>.
- [19] J. Lin, S. T. Pantelides, and W. Zhou, *ACS Nano* **9**, 5189 (2015), ISSN 1936-0851, URL <https://doi.org/10.1021/acsnano.5b00554>.
- [20] F. Yao, Y. Cai, Z. Xiao, G. Zhang, R.-J. Xie, and C. Jin, *2D Mater.* **8**, 025004 (2020), ISSN 2053-1583, URL <https://dx.doi.org/10.1088/2053-1583/abce09>.
- [21] C. Speckmann, A. Angeletti, L. Kyvala, D. Lamprecht, F. Herterich, C. Mangler, L. Filipovic, C. Dellago, C. Franchini, and J. Kotakoski (2024), arXiv:2409.11102, URL <https://arxiv.org/abs/2409.11102v1>.
- [22] A. Yoshimura, M. Lamparski, J. Giedt, D. Lingerfelt, J. Jakowski, P. Ganesh, T. Yu, B. G. Sumpter, and V. Meunier, *Nanoscale* **15**, 1053 (2023), URL <https://pubs.rsc.org/en/content/articlelanding/2023/nr/d2nr01018f>.
- [23] G. Algara-Siller, S. Kurasch, M. Sedighi, O. Lehtinen, and U. Kaiser, *Appl. Phys. Lett.* **103**, 203107 (2013), ISSN 0003-6951, URL <https://aip.scitation.org/doi/10.1063/1.4830036>.
- [24] T. Lehnert, O. Lehtinen, G. Algara-Siller, and U. Kaiser, *Appl. Phys. Lett.* **110**, 033106 (2017), ISSN 0003-6951, URL <https://aip.scitation.org/doi/10.1063/1.4973809>.
- [25] M. Jain, S. Kretschmer, J. Meyer, and A. V. Krasheninnikov, *Phys. Rev. Mater.* **8**, 054004 (2024), URL <https://link.aps.org/doi/10.1103/PhysRevMaterials.8.054004>.
- [26] M. Quincke, M. Mundsinger, J. Biskupek, and U. Kaiser, *Nano Lett.* **24**, 10496 (2024), ISSN 1530-6984, URL <https://doi.org/10.1021/acs.nanolett.4c02391>.
- [27] Y.-C. Lin, D. O. Dumcenco, Y.-S. Huang, and K. Suenaga, *Nat. Nanotechnol.* **9**, 391 (2014), ISSN 1748-3395, URL <https://www.nature.com/articles/nnano.2014.64>.
- [28] Q. Chen, H. Li, S. Zhou, W. Xu, J. Chen, H. Sawada, C. S. Allen, A. I. Kirkland, J. C. Grossman, and J. H. Warner, *ACS Nano* **12**, 7721 (2018), ISSN 1936-0851, URL <https://doi.org/10.1021/acsnano.8b01610>.
- [29] J. Chen, S. Zhou, Y. Wen, G. H. Ryu, C. Allen, Y. Lu, A. I. Kirkland, and J. H. Warner, *Nanoscale* **11**, 1901 (2019), ISSN 2040-3372, URL <https://pubs.rsc.org/en/content/articlelanding/2019/nr/c8nr08821g>.
- [30] H. Inani, D. H. Shin, J. Madsen, H. Jeong, M. H. Kwon, N. McEvoy, T. Susi, C. Mangler, S. W. Lee, K. Mustonen, et al., *Adv. Funct. Mater.* **31**, 2008395 (2021), ISSN 1616-301X, URL <https://onlinelibrary.wiley.com/doi/full/10.1002/adfm.202008395>.
- [31] S. Li, J. Lin, Y. Chen, Z. Luo, H. Cheng, F. Liu, J. Zhang, and S. Wang, *Small* **20**, 2303511 (2024), ISSN 1613-6810, URL <https://onlinelibrary.wiley.com/doi/10.1002/smll.202303511>.
- [32] Q. Chen, H. Li, W. Xu, S. Wang, H. Sawada, C. S. Allen, A. I. Kirkland, J. C. Grossman, and J. H. Warner, *Nano Lett.* **17**, 5502 (2017), ISSN 1530-6984, URL <https://doi.org/10.1021/acs.nanolett.7b02192>.
- [33] H.-P. Komsa, S. Kurasch, O. Lehtinen, U. Kaiser, and A. V. Krasheninnikov, *Phys. Rev. B* **88**, 035301 (2013), URL <https://link.aps.org/doi/10.1103/PhysRevB.88.035301>.

- 1103/PhysRevB.88.035301.
- [34] H.-P. Komsa and A. V. Krasheninnikov, Phys. Rev. B **91**, 125304 (2015), URL <https://link.aps.org/doi/10.1103/PhysRevB.91.125304>.
- [35] M. Precner, T. Polaković, Q. Qiao, D. J. Trainer, A. V. Putilov, C. Di Giorgio, I. Cone, Y. Zhu, X. X. Xi, M. Iavarone, et al., Sci. Rep. **8**, 6724 (2018), ISSN 2045-2322, URL <https://www.nature.com/articles/s41598-018-24913-y>.
- [36] A. Chirita, A. Markevich, M. Tripathi, N. A. Pike, M. J. Verstraete, J. Kotakoski, and T. Susi, Phys. Rev. B **105**, 235419 (2022), URL <https://link.aps.org/doi/10.1103/PhysRevB.105.235419>.
- [37] P. Chen, W. Xu, Y. Gao, P. Holdway, J. H. Warner, and M. R. Castell, J. Phys. Chem. C **123**, 3876 (2019), ISSN 1932-7447, URL <https://doi.org/10.1021/acs.jpcc.8b11298>.
- [38] S. Ahmad and S. Mukherjee, Graphene **03**, 52 (2014), ISSN 2169-3439, 2169-3471, URL <http://www.scirp.org/journal/doi.aspx?DOI=10.4236/graphene.2014.34008>.
- [39] A. Postl, P. P. P. Hilgert, A. Markevich, J. Madsen, K. Mustonen, J. Kotakoski, and T. Susi, Carbon **196**, 596 (2022), ISSN 0008-6223, URL <https://www.sciencedirect.com/science/article/pii/S0008622322004079>.
- [40] Y. Han, T. Hu, R. Li, J. Zhou, and J. Dong, Phys. Chem. Chem. Phys. **17**, 3813 (2015), ISSN 1463-9084, URL <https://pubs.rsc.org/en/content/articlelanding/2015/cp/c4cp04319g>.
- [41] S. Wang, G.-D. Lee, S. Lee, E. Yoon, and J. H. Warner, ACS Nano **10**, 5419 (2016), ISSN 1936-0851, URL <https://doi.org/10.1021/acsnano.6b01673>.
- [42] C. Gao, X. Yang, M. Jiang, L. Chen, Z. Chen, and C. V. Singh, Phys. Chem. Chem. Phys. **23**, 19525 (2021), ISSN 1463-9084, URL <https://pubs.rsc.org/en/content/articlelanding/2021/cp/d1cp02852a>.
- [43] M. O'Brien, N. McEvoy, T. Hallam, H.-Y. Kim, N. C. Berner, D. Hanlon, K. Lee, J. N. Coleman, and G. S. Duesberg, Sci. Rep. **4**, 7374 (2014), ISSN 2045-2322, URL <https://www.nature.com/articles/srep07374>.
- [44] J. C. Meyer, C. O. Girit, M. F. Crommie, and A. Zettl, Appl. Phys. Lett. **92**, 123110 (2008), ISSN 0003-6951, URL <https://doi.org/10.1063/1.2901147>.
- [45] A. Trentino, J. Madsen, A. Mittelberger, C. Mangler, T. Susi, K. Mustonen, and J. Kotakoski, Nano Lett. **21**, 5179 (2021), ISSN 1530-6984, URL <https://doi.org/10.1021/acs.nanolett.1c01214>.